Research Article Vol. 6, No. 2 / February 2019 / Optica 160

Generating few-cycle radially polarized pulses

Fanqi Kong,[1] Hugo Larocque,[2,3] Ebrahim Karimi,[2] P. B. Corkum,[1,2] and Chunmei Zhang[1,*]

[1]Joint Attosecond Science Lab, University of Ottawa and National Research Council of Canada, Ottawa, Ontario K1A0R6, Canada
[2]Department of Physics, University of Ottawa, Ottawa, Ontario K1N 6N5, Canada
[3]Department of Electrical Engineering and Computer Science, Massachusetts Institute of Technology, Cambridge, Massachusetts 02139, USA
*Corresponding author: chunmei.zhang@uottawa.ca

Received 25 September 2018; revised 22 December 2018; accepted 25 December 2018 (Doc. ID 345986); published 30 January 2019

A radially polarized beam is axially symmetric and is able to produce tightly focused light fields beyond the Gaussian beam diffraction limit. However, with the current technology, its duration is limited by the relatively narrow bandwidth that the generation techniques can support. Using a 10 cycle pulse with a central wavelength of 1.8 μm, we show that radially polarized beams can be compressed to the few-cycle regime, while still maintaining their radially polarized nature. Therefore, it seems feasible, using only well-developed methods, to reach focused intensities of $\sim 10^{19}$ W/cm^2. Conversion via high-harmonic generation will also open a route for applications in attosecond science, especially for a wide range of optical measurements and optical control that require high spatial and high temporal resolution.

https://doi.org/10.1364/OPTICA.6.000160

1. INTRODUCTION

Vector beams are laser beams with a nonuniform polarization structure across their profile; a subclass of them has an intensity and polarization profile that is cylindrically symmetric [1]. Cylindrical vector beams have been extensively investigated during the past years in different application fields such as optical trapping [2], high-resolution imaging [3], laser machining [4], laser acceleration [5,6], and communications [7]. An important characteristic of a tightly focused radially polarized beam, for example, is that it forms a smaller focus spot than what can be achieved with a comparable beam of either linear or circular polarization [8].

Many methods produce cylindrical vector beams—especially radially and azimuthally polarized beams. There are intracavity devices [9] for lasers that efficiently convert a conventional single-mode Gaussian laser beam into one with a different polarization distribution [10,11]. However, these devices always have a relatively narrow bandwidth.

In all areas of ultrafast science, pulses can be amplified or shaped up to the bandwidth limit of the most narrowband processes involved and then compressed by self-phase-modulation in a nonlinear medium—often a fiber. This is how the high-power few-cycle pulses used for attosecond science are created [12]. This method can also create single-cycle pulses in the visible or near-IR [13,14]. Optical pulse compression by self-phase-modulation is a critical element in all ultrashort pulse lasers [15]. In fact, optical continua can even be generated by self-phase-modulation in fibers with noble gases [16,17]. In all of these cases, the final pulse duration can be much shorter than what the bandwidth restriction might imply.

In this paper, our aim is to show that pulse compression is available for cylindrically symmetric vector beams. Pulse compression will greatly expand the application area of these beams.

For our experiment, we have chosen a radially polarized beam that we generate using a linearly polarized Gaussian beam propagating through a q-plate [18], and we find very similar results for azimuthal polarization. We will show that the q-plate has a bandwidth limit that is insufficient to create a few-cycle pulse. However, once the pulse is shaped and spatially filtered to ensure its cylindrical symmetry, we will show that it can be compressed down to a few-cycles by means of a conventional gas-filled hollow-core fiber compressor.

2. EXPERIMENTAL SETUP

We use a 1.8 μm beam produced by the laser source, which consists of a chirped-pulse-amplified Ti: Sapphire laser system and a white-light seeded high-energy optical parametric amplifier (HE-TOPAS, Light Conversion) [19]. The Ti: Sapphire laser system that we used provides 50 fs laser pulses at 800 nm with a 5 mJ pulse energy at a repetition rate of 1 kHz. The optical parametric amplifier (OPA) is pumped by the 800 nm light, and it provides 1.8 μm pulses with ~50 fs duration. The 1.8 μm pulses from the OPA are spatially cleaned by focusing into a hollow-core fiber (1.4 m long, 400 μm core diameter) with an $f = 75$ cm lens made of CaF_2.

The spatially filtered beam is then refocused into a krypton-filled hollow-core fiber (20 cm long, 150 μm or 250 μm core diameter) by an $f = 15$ cm or $f = 30$ cm lens, as shown in Fig. 1. The nonlinear propagation in the hollow-core fiber adds bandwidth and an approximately linear positive chirp.

We use a q-plate ($q = 1/2$) for generating a radially polarized beam [18]. A q-plate is composed of two indium tin oxide (ITO) substrates covered by a polyimide layer and a liquid crystal layer. The alignment pattern of the liquid crystals in the q-plate is "written" during its fabrication. Its liquid crystals' optical retardation is controlled through an external electric field, which is applied on

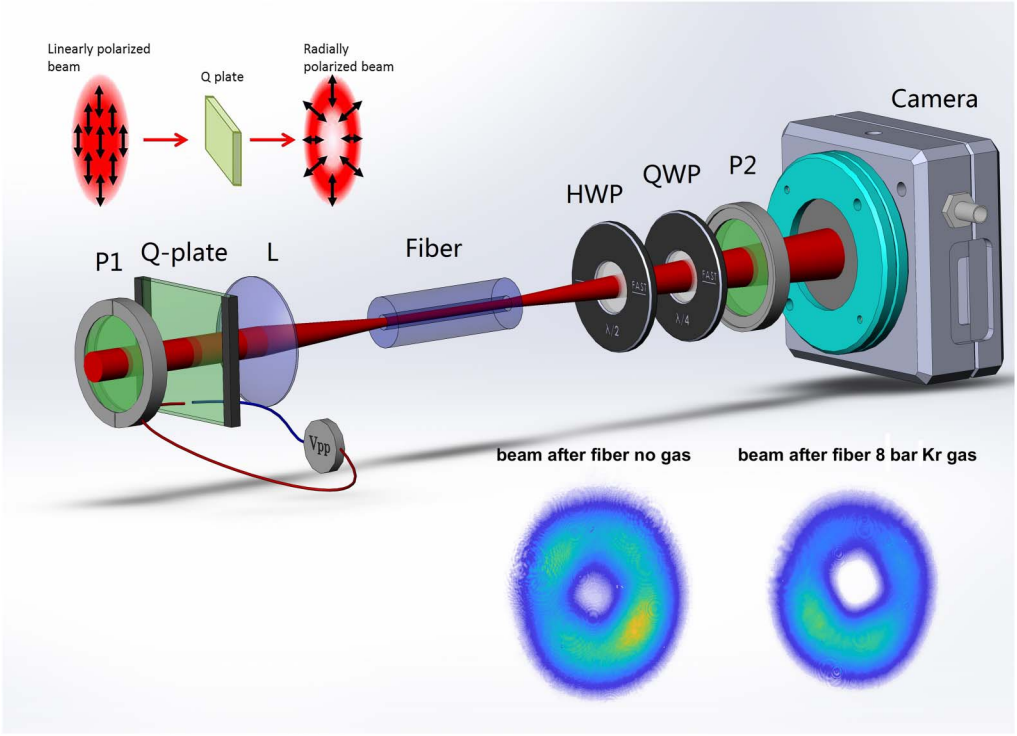

Fig. 1. Setup of a few-cycle vortex beam generation experiment with a 1.8 μm laser source. P1 and P2, polarizers; Vpp, power supply for the *q*-plate; L, lens; HWP, achromatic half-wave plate for the central wavelength of 1.8 μm; QWP, achromatic quarter-wave plate for the central wavelength of 1.8 μm. The fiber is 20 cm long with a 150 μm or 250 μm core. The right lower two figures show the beam profile of the output beams after the fiber is put under vacuum and is filled with 8 bar Kr gas, respectively.

the plate. Therefore, the device's central wavelength can be tuned to a different one by simply adjusting the applied voltage.

However, the *q*-plate can only support a relatively narrow spectrum for a given voltage. In Fig. 2, we compare the polarization of the initial pulse (blue) and the pulse that has passed the *q*-plate (red). We perform this comparison over a broadband infrared spectrum ranging from 1.5 to 2.1 μm and record the pulse's spectrum after it goes through a polarizer with a fiber spectrometer (Ocean Optics, USB 2000+). A *q*-plate fundamentally consists of a structured half-wave plate, such that a passing beam's polarization locally remains linear but is rotated to a degree, depending on the relative angle between the beam's polarization and the local alignment of the liquid crystals. We can make use of this effect to extract the bandwidth that the *q*-plate supports by examining the degree to which linear polarization is preserved throughout our spectrum. This degree of similarity can be measured by making the beam go through a polarizer. Namely, we expect wavelengths that experience the required conversion to remain linear with a 90° rotation and, therefore, not go through the polarizer. To gauge this condition, we use a measure called the "polarization identicality," defined as the minimum output of the polarizer as the polarizer is rotated divided by the maximum output. In Fig. 2, the blue and red curves show the polarization identicality of the beams before and after the *q*-plate, respectively. Only a ∼100 nm bandwidth gets a similar optical retardation and maintains a zero-valued polarization identicality. Therefore, the figure shows that a *q*-plate could not support the full spectrum of a few-cycle [20].

Therefore, we have to use the *q*-plate where the pulse bandwidth is relatively narrow—i.e., before pulse compression. As shown in Fig. 1, a polarizer after the fiber spatial filter is used

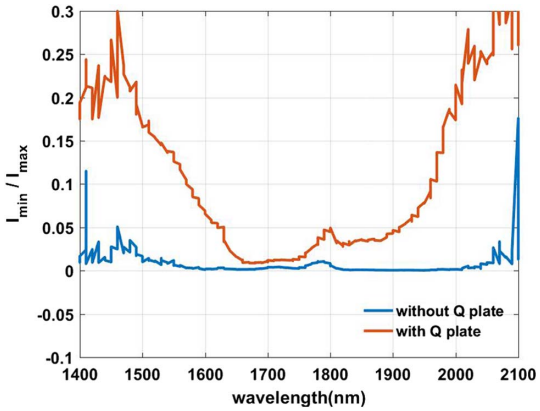

Fig. 2. "Polarization identicality" of the laser beam before and after the *q*-plate. This measure is defined in the text and is an indicator of the conversion efficiency of the *q*-plate at a given wavelength, where values closer to zero indicate a higher efficiency. The blue and red curves show the identicality of the beam before and after the *q*-plate, respectively.

to maintain a homogeneous linear polarization. Then, the beam passes a *q*-plate with a proper bias voltage for the central wavelength of 1.8 μm, and the linear input polarization is transformed into radial polarization. Finally, the radially polarized beam is spectrally broadened in the fiber. In Fig. 1, the right lower two figures show the beam profiles of the output beams after the fiber under vacuum and the fiber filled with 8 bar krypton gas, respectively. We can see that the beam has a uniform doughnut-shaped intensity profile and is not distorted by passing the hollow-core fiber when it is used passively or when it is filled with krypton gas.

3. RESULTS

For our experiment, the Gaussian beam on the q-plate has an energy of 200 μJ within a ~5.5 mm FWHM beam diameter. Using a radially polarized beam with an input energy of 150 μJ, we achieved 40% transmission. In comparison, the transmission for the Gaussian beam is 47% (using the same coupling geometry). The highest energy we used on the q-plate is 220 μJ. Therefore, the damage threshold of the q-plate is higher than 1.85×10^{10} W/cm^2.

In the krypton-filled hollow-core fiber, the spectrum of the pulse is broadened by self-phase modulation. Figure 3(a) shows the broadened spectrum for four segments of the beam selected from different quadrants of the doughnut. The spectra of the lower, left, and right parts of the beam have a similar bandwidth, while that of the upper part is a little broader.

We know from conventional fiber compression that a pulse that exits a fiber is chirped and, therefore, we compensate for the chirp with an antireflection-coated fused silica plate in the beam path [21] before characterizing the beam's temporal duration with a second-harmonic-generation (SHG) frequency-resolved optical gating (FROG). The temporal profiles of the amplitude and phase of different quadrants of the shortened pulses are shown in Figs. 3(b)–3(e). These curves correspond to 15 fs pulses for the upper part of the beam and 17 fs pulses for the remaining three parts. All are less than three optical cycles in duration and have a central wavelength of 1.8 μm.

It is not sufficient to show that the compressed pulse is short. We must also confirm its polarization state. We measure the polarization state of the output-broadened beam by passing the beam through a polarizer and recording the beam profile using a camera. For a radially polarized beam, after the polarizer, the output beam will be a linearly polarized beam with polarization parallel to the transmission axis of the polarizer. The output electric field strength will have its peak at the polarizer's orientation angle. As shown in Fig. 4, the intensity profile has two lobes that rotate with the orientation of the polarizer, which is indicated by red arrows [Figs. 4(b) to 4(e)]. Therefore, the beam is always oriented with the radial direction along the polarizer axis. This confirms that the output-broadened beam is still a cylindrical vector beam with radial polarization.

We also characterized the topological charge of the compressed beam. For beams with phase singularities, the topological charge is quantified by recording the interference between the beam and a tilted Gaussian, thus resulting in a forked interference pattern [22]. The difference in the number of interference fringes between one side and the other corresponds to the topological charge of the singularity. This procedure can be simplified by using a collinear interferometer instead.

Now consider the radially polarized beam from the orbital angular momentum (OAM) perspective. A radially polarized beam is a beam that can be considered to be a superposition of left and right circularly polarized components with a phase delay around the circumference. The required phase delay corresponding to the two beams having opposite values of helicity and $|\mathrm{OAM}| = 1$. The Jones matrix expression of a radially polarized beam with an azimuthal phase $\exp(i\varphi)$ can be written as

$$\begin{pmatrix}\cos\varphi\\ \sin\varphi\end{pmatrix} = \frac{1}{2}e^{-i\varphi}\cdot\begin{pmatrix}1\\ i\end{pmatrix} + \frac{1}{2}e^{i\varphi}\cdot\begin{pmatrix}1\\ -i\end{pmatrix}, \tag{1}$$

which consists of a right-hand circularly polarized (RHCP) beam and a left-hand circularly polarized (LHCP) beam with opposite helicities and opposite topological charges, where φ is the azimuthal coordinate angle in the plane perpendicular to the propagation.

If this beam passes through a quarter-wave plate, the two circularly polarized components identified above will be converted into two perpendicular linearly polarized beams. Then, a polarizer will interfere with the two components when we select a given polarization direction. Assuming the quarter-wave plate and polarizer are both along the x axis, we should observe the interference signal below:

$$\begin{pmatrix}\cos\varphi\\ \sin\varphi\end{pmatrix} \begin{matrix}\nearrow \frac{1}{2}e^{-i\varphi}\cdot\begin{pmatrix}1\\ i\end{pmatrix} \overset{\lambda/4}{\Rightarrow} \frac{1}{2}e^{-i\varphi}\cdot\begin{pmatrix}1\\ -1\end{pmatrix} \overset{P}{\Rightarrow} \frac{1}{2}e^{-i\varphi}\cdot\begin{pmatrix}1\\ 0\end{pmatrix}\searrow \\ \searrow \frac{1}{2}e^{i\varphi}\cdot\begin{pmatrix}1\\ -i\end{pmatrix} \overset{\lambda/4}{\Rightarrow} \frac{1}{2}e^{i\varphi}\cdot\begin{pmatrix}1\\ 1\end{pmatrix} \overset{P}{\Rightarrow} \frac{1}{2}e^{i\varphi}\cdot\begin{pmatrix}1\\ 0\end{pmatrix}\nearrow \end{matrix} \cos\varphi\cdot\begin{pmatrix}1\\ 0\end{pmatrix}, \tag{2}$$

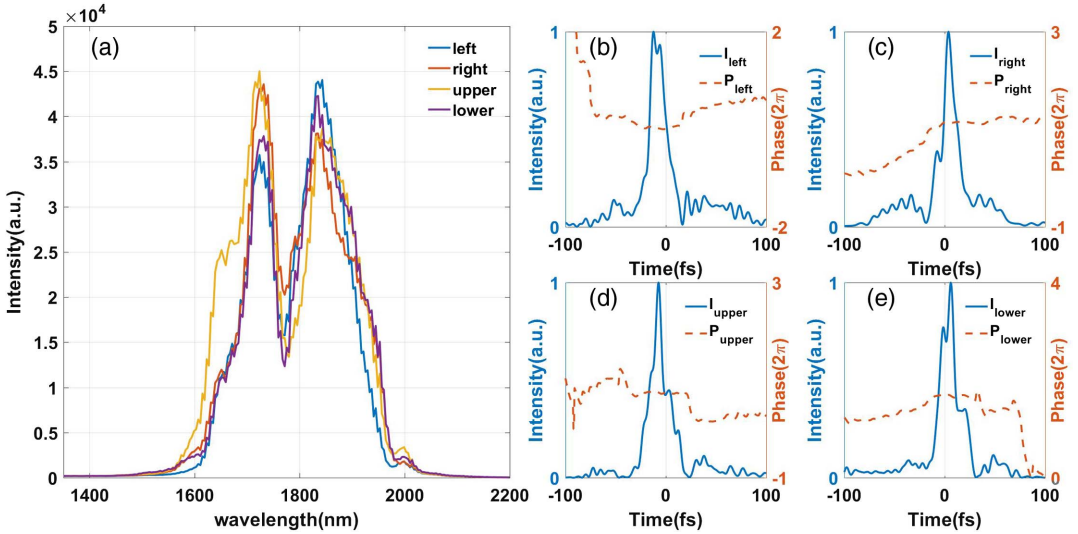

Fig. 3. Compression of the radially polarized beam. (a) Spectra of the spatially polarized beam measured at four different spatial locations after the fiber compressor. The spectra of the lower, left, and right parts are similar, and the upper spectrum is a little broader than the others. (b–e) Temporal profiles (blue curves) and phases (red curves) of the laser fields corresponding to the four spectra in (a), measured using a FROG. The pulse durations of the lower, left, and right parts are 17 fs, and that of the upper part is 15 fs, which agree with their bandwidths.

where we considered a quarter-wave plate oriented at 0°. Finally, if we insert a half-wave plate between the q-plate and the quarter-wave plate, the half-wave plate flips the handedness of the circularly polarized beams and also shifts the relative phases of the beams. Assuming the angle that the fast axis of the half-wave plate makes with respect to the x axis is θ, the Jones vector expression for the whole setup is

$$\begin{pmatrix}\cos\varphi\\ \sin\varphi\end{pmatrix} \begin{matrix}\nearrow \frac{1}{2}e^{-i\varphi}\cdot\begin{pmatrix}1\\ i\end{pmatrix}\overset{\lambda/2}{\Rightarrow}\frac{1}{2}e^{-i\varphi}\cdot e^{i2\theta}\cdot\begin{pmatrix}1\\ -i\end{pmatrix}\overset{\lambda/4}{\Rightarrow}\frac{1}{2}e^{-i\varphi}\cdot e^{i2\theta}\cdot\begin{pmatrix}1\\ 1\end{pmatrix}\overset{P}{\Rightarrow}\frac{1}{2}e^{-i\varphi}\cdot e^{i2\theta}\cdot\begin{pmatrix}1\\ 0\end{pmatrix}\searrow\\ \searrow \frac{1}{2}e^{i\varphi}\cdot\begin{pmatrix}1\\ -i\end{pmatrix}\overset{\lambda/2}{\Rightarrow}\frac{1}{2}e^{i\varphi}\cdot e^{-i2\theta}\cdot\begin{pmatrix}1\\ i\end{pmatrix}\overset{\lambda/4}{\Rightarrow}\frac{1}{2}e^{i\varphi}\cdot e^{-i2\theta}\cdot\begin{pmatrix}1\\ -1\end{pmatrix}\overset{P}{\Rightarrow}\frac{1}{2}e^{i\varphi}\cdot e^{-i2\theta}\cdot\begin{pmatrix}1\\ 0\end{pmatrix}\nearrow\end{matrix} \cos(\varphi-2\theta)\cdot\begin{pmatrix}1\\ 0\end{pmatrix}, \tag{3}$$

Thus, the half-wave plate gives a positive 2θ phase delay to the left circular polarized beam and a negative 2θ phase delay to the right circular polarized beam. Therefore, we should observe a $\pm 2\theta$ phase delay for the two linearly polarized beams and the two arms of the linear interferometer.

As we rotate the half-wave plate, the relative phase between the two arms of the interferometer will be changed accordingly. The relative phase change is 4 times the phase delay corresponding to the rotated angle of the half-wave plate. During a full scan of the wave plate, the phase delay between the interferometer arms will be 4 times the phase gradient of the beam's wavefront. Therefore, the period number of the interference signal for a full circle scan of the half-wave plate also gives the topological charge.

To demonstrate this alternative approach, we recorded the beam profile with the CCD camera as a function of the rotation angle of the half-wave plate, as shown in Fig. 1. We obtain a two-lobe intensity pattern, similar to the pattern obtained by passing through a polarizer (Fig. 4). When the half-wave plate is rotated, the two-lobe pattern rotates accordingly. Figure 5(a) shows the sum of all the beam intensity patterns for a full 360° scan. Alternatively, we can select one $\delta\phi$-wide segment of the beam and record the signal as the half-wave plate is rotated. We plot the beam energy in this segment as a function of the rotation angle of the half-wave plate in Fig. 5(b). We obtain four peaks for a full 360° scan, indicating that the phase changes by 2π for a full 360° wave plate scan. In addition, if we check the points with 180° separation, they show the same peak position—the intensity profile does not distinguish between π phase differences.

We retrieve the phase of each point on the circle with 2° resolution and plot it as the function of the point angle in Fig. 5(c). The curve confirms the 2π phase shift of the beam wavefront for the full 360° scan of the half-wave plate, corresponding to the topological charge equaling one.

These pulses will have broad applications in high-field physics, and we confirm the focus beam profile of these pulses to estimate the performance of the compressed beam. We have focused the compressed pulses with an $f = 75$ mm CaF_2 lens, and the profile is shown in Fig. 5(d). The beam diameter is ~60 μm. With a 15 fs pulse duration and 60 μJ energy, we can estimate the peak intensity to be $>1.4\times10^{14}$ W/cm^2.

In our experiment, the beam energy is limited by the laser and the size of the q-plate we used, which is ~5 mm. Had we used a larger q-plate and a high-energy OPA, the energy and peak intensity could have been higher. In fact, S-waveplates [23,24], a relative of q-plates made by cracking quartz, will withstand a much higher intensity. The current limiting factor is hollow-core pulse compression with an experimental limit to the output of ~5 mJ.

A 5 mJ pulse [25] with a pulse duration of 15 fs has a peak power of 3×10^{11} W. Focused to the wavelength scale, an intensity of 10^{19} W/cm^2 is feasible. This would be a very interesting pulse with a longitudinal field reaching relativistic intensities. Long before such an intensity, high harmonics can be created in gases and solids, opening a new regime of attosecond science.

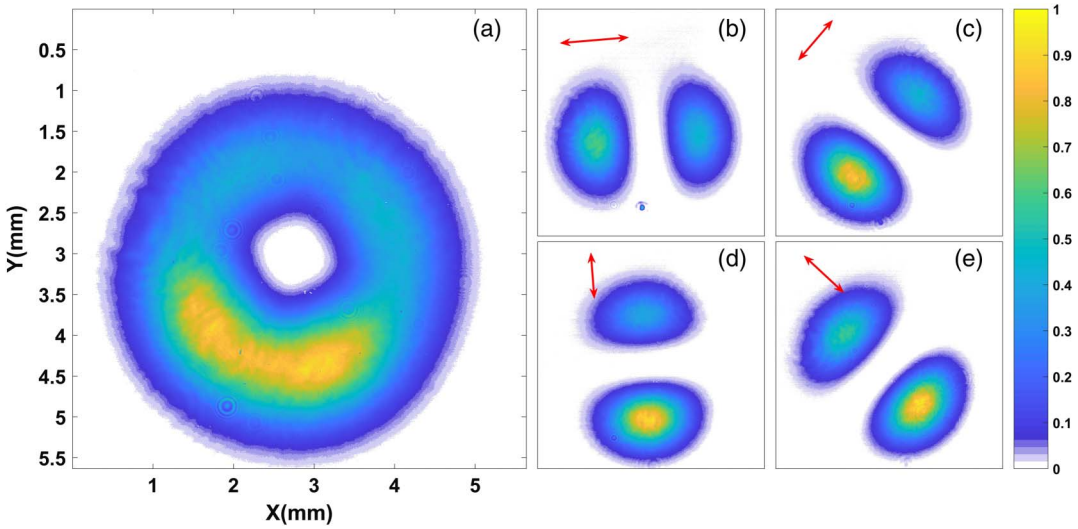

Fig. 4. Polarization measurement of the radially polarized beam. (a) Beam profile without polarization selection. (b–e) Beam profiles upon propagation through a polarizer, measured with a CCD camera for four different axis angles.

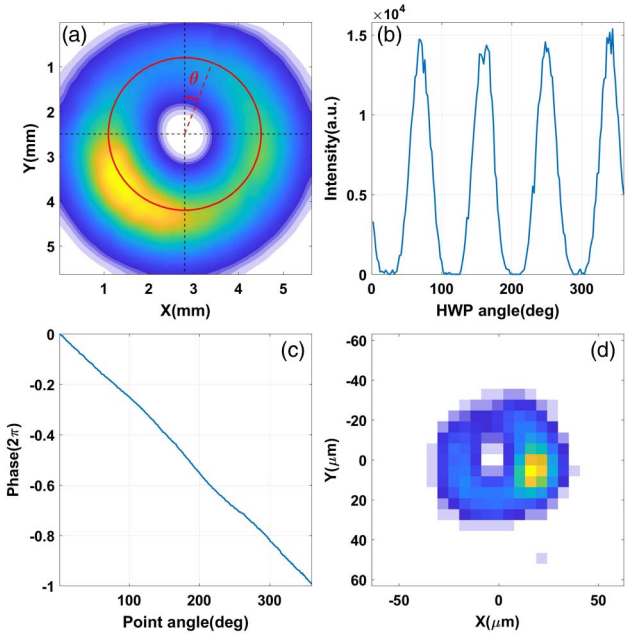

Fig. 5. Wavefront interference scan and the focus beam profile. (a) Integrated intensity profiles for a full 360° scan. (b) Interference signal for one point of the beam as a function of HWP angle. (c) Phase retrieved for different points on the circle's circumference. (d) Focus beam profile of the compressed radially polarized beam.

4. CONCLUSION

In conclusion, we have used a gas-filled hollow-core fiber to compress a radially polarized vector beam in the same way that we compress Gaussian beams. While we employed 1.8 μm light for this demonstration, we expect that hollow-core fiber compression will be possible for other wavelengths and that it can be generalized to more complex fibers. Pulse compression should be possible for any cylindrically symmetric vector beam, and we expect that vector-beam pulse compression can be generalized to single- [26] or multi-plate pulse compression [27] as well.

These pulses will be important for laser acceleration experiments [6] as well as for high-harmonic or attosecond pulse experiments with radially polarized drivers. Using solid or gas as a nonlinear medium, it will be possible to produce radially polarized harmonics with a curved wavefront [28] that will reach wavelength-scale focal spots compared to Gaussian beams [29], thus opening a route towards vacuum ultraviolet (VUV) microscopy.

Funding. Canada Research Chairs; Canada Foundation for Innovation (CFI); Ontario Research Foundation (ORF); Defense Advanced Research Projects Agency (DARPA) (D18AC00011).

Acknowledgment. The authors acknowledge the invaluable engineering assistance of Yu-Hsuan Wang, as well as important discussions with P. Russell, D. Novoa, and F. Tani from the Max Planck Institute for the Science of Light.

REFERENCES

1. Q. Zhan, "Cylindrical vector beams: from mathematical concepts to applications," Adv. Opt. Photon. **1**, 1–57 (2009).
2. B. J. Roxworthy and K. C. Toussaint, Jr., "Optical trapping with π-phase cylindrical vector beams," New J. Phys. **12**, 073012 (2010).
3. R. Chen, K. Agarwal, C. J. R. Sheppard, and X. Chen, "Imaging using cylindrical vector beams in a high-numerical-aperture microscopy system," Opt. Lett. **38**, 3111–3114 (2013).
4. M. Meier, V. Romano, and T. Feurer, "Material processing with pulsed radially and azimuthally polarized laser radiation," Appl. Phys. A **86**, 329–334 (2007).
5. B. Hafizi, E. Esarey, and P. Sprangle, "Laser-driven acceleration with Bessel beams," Phys. Rev. E **55**, 3539–3545 (1997).
6. C. Varin, S. Payeur, V. Marceau, S. Fourmaux, A. April, B. Schmidt, P.-L. Fortin, N. Thiré, T. Brabec, F. Légaré, J.-C. Kieffer, and M. Piché, "Direct electron acceleration with radially polarized laser beams," Appl. Sci. **3**, 70–93 (2013).
7. G. Milione, T. A. Nguyen, J. Leach, D. A. Nolan, and R. R. Alfano, "Using the nonseparability of vector beams to encode information for optical communication," Opt. Lett. **40**, 4887–4890 (2015).
8. R. Dorn, S. Quabis, and G. Leuchs, "Sharper focus for a radially polarized light beam," Phys. Rev. Lett. **91**, 233901 (2003).
9. D. Pohl, "Operation of a ruby laser in the purely transverse electric mode TE01," Appl. Phys. Lett. **20**, 266–267 (1972).
10. M. Stalder and M. Schadt, "Linearly polarized light with axial symmetry generated by liquid-crystal polarization converters," Opt. Lett. **21**, 1948–1950 (1996).
11. M. R. Beversluis, L. Novotny, and S. J. Stranick, "Programmable vector point-spread function engineering," Opt. Express **14**, 2650–2656 (2006).
12. M. Nisoli and G. Sansone, "New frontiers in attosecond science," Prog. Quantum Electron. **33**, 17–59 (2009).
13. M. Nisoli, S. De Silvestri, O. Svelto, R. Szipöcs, K. Ferencz, C. Spielmann, S. Sartania, and F. Krausz, "Compression of high-energy laser pulses below 5 fs," Opt. Lett. **22**, 522–524 (1997).
14. B. Schmidt, A. Shiner, P. Lassonde, J. Kieffer, P. Corkum, D. M. Villeneuve, and F. Légaré, "CEP stable 16 cycle laser pulses at 18 μm," Opt. Express **19**, 6858–6864 (2011).
15. W. J. Tomlinson, R. H. Stolen, and C. V. Shank, "Compression of optical pulses chirped by self-phase modulation in fibers," J. Opt. Soc. Am. B **1**, 139–149 (1984).
16. M. Nisoli, S. De Silvestri, and O. Svelto, "Generation of high energy 10 fs pulses by a new pulse compression technique," Appl. Phys. Lett. **68**, 2793–2795 (1996).
17. P. B. Corkum, C. Rolland, and T. Srinivasan-Rao, "Supercontinuum generation in gases," Phys. Rev. Lett. **57**, 2268–2271 (1986).
18. H. Larocque, J. Gagnon-Bischoff, F. Bouchard, R. Fickler, J. Upham, R. W. Boyd, and E. Karimi, "Arbitrary optical wavefront shaping via spin-to-orbit coupling," J. Opt. **18**, 124002 (2016).
19. C. Zhang, G. Vampa, D. M. Villeneuve, and P. B. Corkum, "Attosecond lighthouse driven by sub-two-cycle, 1.8 μm laser pulses," J. Phys. B **472**, 6–10 (2015).
20. L. Yan, P. Gregg, E. Karimi, A. Rubano, L. Marrucci, R. Boyd, and S. Ramachandran, "Q-plate enabled spectrally diverse orbital-angular-momentum conversion for stimulated emission depletion microscopy," Optica **2**, 900–903 (2015).
21. B. E. Schmidt, P. Béjot, M. Giguère, A. D. Shiner, C. Trallero-Herrero, É. Bisson, J. Kasparian, J.-P. Wolf, D. M. Villeneuve, J.-C. Kieffer, P. B. Corkum, and F. Légaré, "Compression of 1.8 μm laser pulses to sub two optical cycles with bulk material," Appl. Phys. Lett. **96**, 121109 (2010).
22. F. Kong, C. Zhang, F. Bouchard, Z. Li, G. G. Brown, D. H. Ko, T. J. Hammond, L. Arissian, R. W. Boyd, E. Karimi, and P. B. Corkum, "Controlling the orbital angular momentum of high harmonic vortices," Nat. Commun. **8**, 14970 (2017).
23. M. Beresna, M. Gecevičius, P. G. Kazansky, and T. Gertus, "Radially polarized optical vortex converter created by femtosecond laser nanostructuring of glass," Appl. Phys. Lett. **98**, 201101 (2011).
24. "S-waveplate (Radial Polarization Converter)," Altechna, https://www.altechna.com/products/s-waveplate-radial-polarization-converter/.
25. V. Cardin, N. Thiré, S. Beaulieu, V. Wanie, F. Légaré, and B. E. Schmidt, "0.42 TW 2-cycle pulses at 1.8 μm via hollow-core fiber compression," Appl. Phys. Lett. **107**, 181101 (2015).
26. M. Seidel, G. Arisholm, J. Brons, V. Pervak, and O. Pronin, "All solid-state spectral broadening: an average and peak power scalable method for compression of ultrashort pulses," Opt. Express **24**, 9412–9428 (2016).
27. C.-H. Lu, Y.-J. Tsou, H.-Y. Chen, B.-H. Chen, Y.-C. Cheng, S.-D. Yang, M.-C. Chen, C.-C. Hsu, and A. H. Kung, "Generation of intense supercontinuum in condensed media," Optica **1**, 400–406 (2014).
28. M. Sivis, M. Taucer, G. Vampa, K. Johnston, A. Staudte, A. Y. Naumov, D. M. Villeneuve, C. Ropers, and P. B. Corkum, "Tailored semiconductors for high-harmonic optoelectronics," Science **357**, 303–306 (2017).
29. S. Quabis, R. Dorn, M. Eberler, O. Glöckl, and G. Leuchs, "Focusing light into a tighter spot," Opt. Commun. **179**, 1–7 (2000).